Publ. Natl. Astron. Obs. Japan Vol. 13. 71 − 81 (2010)

# PSF Analysis of 7 Years' Subaru/Suprime-Cam Data

Sachiyo NODA, Junko FURUSAWA, Reiko FURUSHO, Yoshihiko YAMADA,
Hisanori FURUSAWA, Tomohiko OZAWA*, Tadafumi TAKATA, and Shin-ichi ICHIKAWA

(Received 2010 Nov. 8; accepted 2011 Jan. 11)

**Abstract**

We investigate time variations in Point Spread Function (PSF) for seven years' Subaru/Suprime-Cam data which have been obtained with old CCDs (MIT/LL) and stored in SMOKA (Subaru Mitaka Okayama Kiso Archive system) database[1]. We use the observation frames taken with the Rc, i' or z' filter. Source detections and PSF measurements are performed for observational frames. The seasonal variation of PSF size in a year indicates that the observational condition is better in August - October rather than in March. We also discuss long-term variations and nightly time-to-time variations for PSF size and ellipticity.

Key words: data quality assurance, PSF analysis, archived data, Subaru/Suprime-Cam.

## 1. Introduction

SMOKA (Subaru Mitaka Okayama Kiso Archive system) supplies public science data from Subaru Telescope (Kaifu 1998), 188cm telescope at Okayama Astrophysical Observatory[2], 105cm Schmidt telescope at Kiso Observatory (University of Tokyo)[3], MITSuME telescopes (Kotani et al. 2005) of Tokyo Institute of Technology, and KANATA Telescope (Uemura et al. 2006) at Higashi-Hiroshima Observatory (Hiroshima University). Development and operations of SMOKA are carried out by the Astronomy Data Center (ADC) of the National Astronomical Observatory of Japan (NAOJ) (Baba et al. 2002; Yamamoto et al. 2003; Enoki et al. 2004; Ideta et al. 2005; Yamada et al. 2009).

The Subaru telescope is an optical-infrared telescope whose primary mirror has 8.2m effective aperture at the top of Mauna Kea (4,200 m) in Hawaii. Suprime-Cam is the wide-field camera installed at the prime focus of the Subaru Telescope. In the first light of 1999, observations started with mixed CCD devices, Tektronix Tk2048E and CCID-20 supplied by SITe and MIT Lincoln Laboratory (MIT/LL). All 10 CCDs were replaced with MIT/LL CCDs in 2001 April and cover a wide field of view, 27 arcmin × 34 arcmin with a resolution of 0". 202 pixel$^{-1}$. Details of the Suprime-Cam are given in Miyazaki et al. (2002). The number of refereed papers based on the SMOKA archived data has been increased. More than 70% of those are written using Subaru/Suprime-Cam data. The Suprime-Cam data is clearly the most popular in the SMOKA archived data.

For archive users, it is very important to know the characteristics of the observational data. For example, the long-term, seasonal and time variations of the data provide useful information for them. Also such information is supposed to help general observers creating observation plan. Actually a seasonal trend of PSF size variations from images of Auto Guider (AG, effective wavelength is at 600 nm) is suggested by Miyashita et al. (2004). They found that the PSF size is smallest in September using images of focus check during May 2000 to April 2004. The prototype system of the data quality assurance for the Subaru/Suprime-Cam data which are archived in SMOKA has been reported in Nakata et al. (2005). We aim at more detailed investigation of a long-term, seasonal, and time variations of the Suprime-Cam data by using much larger sample than that used in the study by them, in the course of the quality evaluation of SMOKA archived data.

In this study, the PSF analysis of the Suprime-Cam data for 7 years is presented. The selection of observation frames is explained in section 2. In section 3, we evaluate PSF size and ellipticity. In section 4, the seasonal PSF variations of the archived Subaru/Suprime-Cam data are examined, then long-term and time variations in the PSF are discussed.

## 2. Selection of the Observation Frames

In this study, we utilize Suprime-Cam raw data archived in SMOKA. A large number of sample frame is necessary to investigate long-term, seasonal and time variations in the PSF of the Suprime-Cam images. We apply the following conditions for picking up as many appropriate frames as

* Misato Observatory
[1] http://smoka.nao.ac.jp/
[2] http://www.oao.nao.ac.jp/
[3] http://ioa.s.u-tokyo.ac.jp/kisohp/

possible in an automated manner before PSF evaluation.

Firstly, frames observed during May 2001 - June 2008 are selected. This cut eliminate effects of the CCD chip differences, since the installed chips were all MIT/LL CCDs and their positions in the dewar have been fixed throughout that period.

Secondly, we select filters. Figure 1 gives the total number of observed shots for each filter which has been applied to Suprime-Cam in the period. Here, 'shot' means one-exposure data composed of 10 CCD FITS images. The most popular filter is Rc (W－C－RC, the wavelength range is 592-708 nm), next to i' (W－S－I＋, the wavelength range is 690-844 nm), then z' (W－S－Z＋, the wavelength range is 845-988 nm). Their sensitivities are given in the Subaru web page[4]. We consider the shots taken with such three filters. The number of shots are 7,336, 6,695, and 6,646 for the Rc, i' and z' filters, respectively.

Thirdly, the shots which are supposed to contain point sources are extracted by referring to SMOKA database. We require that 'Data type' in SMOKA should be 'OBJECT'. Also 'Object Name' should not contain following words; 'dome', 'flat', 'focus', 'twilight', 'dark', and 'test'. The numbers of shots are 5,315, 5,504, 5,238 for the Rc, i' and z' filters, respectively.

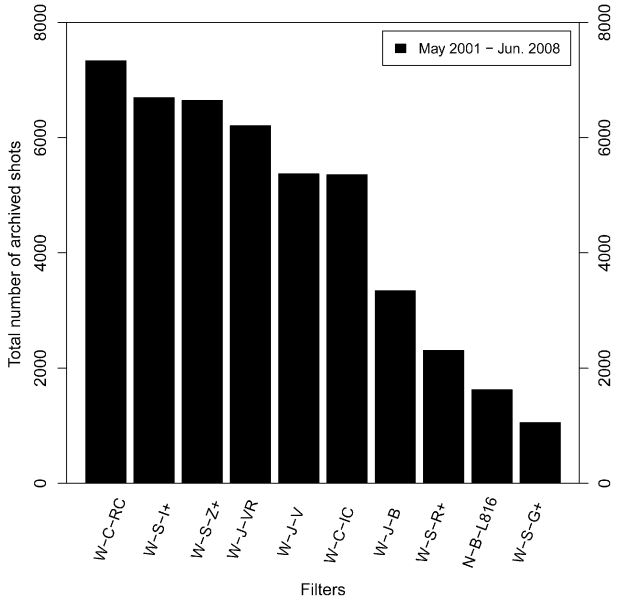


**Fig. 1.** The total number of archived shots for each filter during May 2001 to June 2008. The number of W-C-RC (Rc), W－S－I＋ (i') and W－S－Z＋(z') are the top three fractions of all the archived data.

[4] http://www.naoj.org/Observing/Instruments/SCam/sensitivity_mit.html

## 3. PSF Evaluations of Each Observed Shot

In this study, variations of PSF size and ellipticity are considered as parameters of PSF evaluations. We use the SExtractor software (Bertin and Arnouts 1996) on each frame of the selected shots described in section 2 in order to detect sources and to evaluate PSFs. The SExtractor version is 2.8.6. In the parameter file of SExtractor, DETECT_MINAREA and BACKPHOTO_TYPE are set to 20 and GLOBAL, respectively. Also MAG_ZEROPOINT, PIXEL_SCALE are set to 25.0, 0.2. The others are set to the default values. Figure 2 summarizes the procedure of PSF evaluations. The measurement of PSFs consists of two separate executions of SExtractor ((1) and (2) in figure 2) and associated statistical catalog operations. In this figure, the first execution of SExtractor is carried out with an initial value, SEEING_FWHM＝1.0 arcsec. Detection threshold is set to the 5 sigma of the sky background fluctuations. The two-times executions of SExtractor is necessary to select point sources by SExtractor, because the PSF size can not been evaluated correctly in the case the actual seeing is extremely different from the common initial value.

After the first execution, the objects which are inappropriate for the PSF evaluation are excluded by the following conditions:

(1) The detected object is located at the CCD edges (x < 100, 1950 < x, y < 100, or 4000 < y),
(2) The peak CCD count above the background level is out of the range between 2000 and 25000 counts, or
(3) 'FLAGS' given by SExtractor is not zero. This is the flag showing if an object is saturated, affected by the neighboring objects, or truncated at the CCD edge.

The restriction of (2) is set to eliminate objects which have potentially too small S/N or too large deviation from the CCD linearity. The frames which contain less than 5 effective

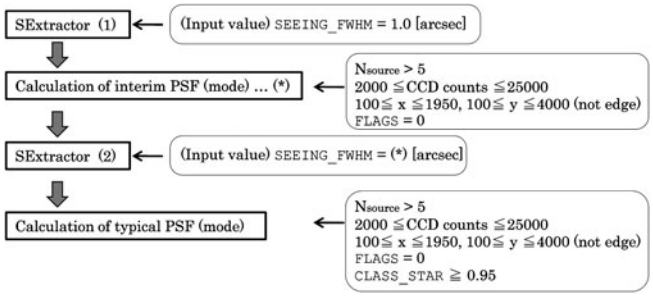


**Fig. 2.** The process of PSF measurements. We execute SExtractor twice. The first execution is performed with the same input value, 1.0 arcsec, while the second one is done with the interim PSF size calculated using the first output.

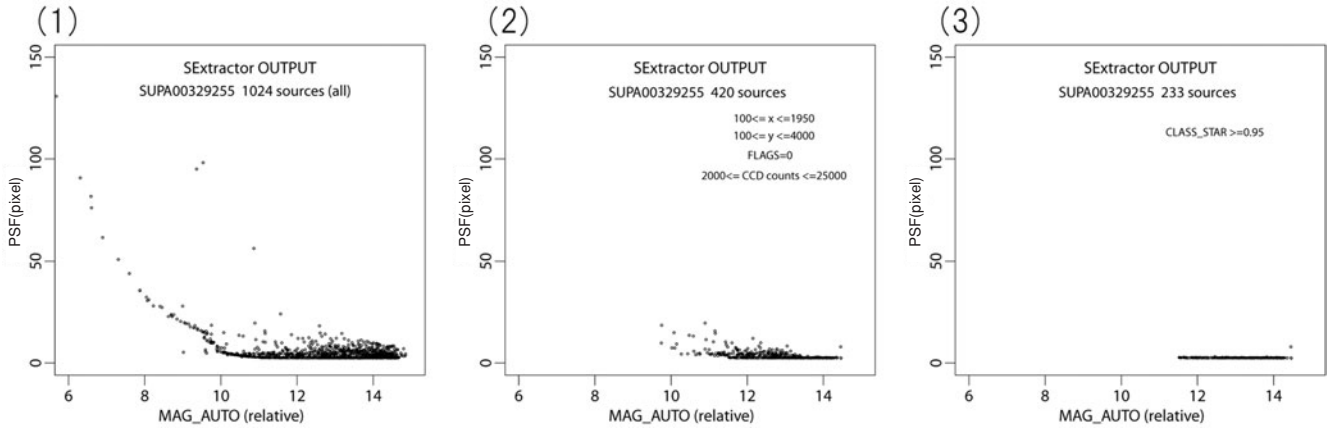


**Fig. 3.** An example of relative Magnitude-PSF(pixel) diagram of SUPA00329255 after the second SExtractor execution. The horizontal axis, 'MAG_AUTO', indicates relative magnitude, whose zero-point is applied in SExtractor. The source is darker as 'MAG_AUTO' is larger. The vertical axis, PSF size (pixel), expresses 'FWHM_IMAGE' computed by SExtractor. The frame, SUPA00329255, was observed on 18 April 2004, on the field of a cluster of galaxies A2390, with 180.0 seconds exposure using Rc filter. The calculated modes of PSF size and ellipticity are 0.52+/-0.02 arcsec and 0.04 +/- 0.03, respectively.
(1) 1,024 sources are detected by the second SExtractor execution.
(2) 420 sources are remained after the cuts of location, FLAG, and CCD counts. The sources are not located at the edge of CCD. Also 'FLAGS' is required to be zero, which means a 'clean source', with in the range of 2,000-25,000 CCD counts.
(3) 233 sources with CLASS_STAR (stellarity) $\geqq$0.95 are finally used for the mode calculation of the frame.
We regard the values as typical PSF size and ellipticity of the frame (3).

objects (likely point sources) are not used in the following aralysis. The mode of PSF size (in pixel) of each frame is computed using the parameter 'FWHM_IMAGE' given by SExtractor. The calculated PSF size in arcsec (the mode of PSF size in pixel $\times$ 0". 202) is used as an input parameter, SEEING_FWHM, in the second execution of SExtractor. After the second execution, we require large stellarity index (CLASS_STAR $\geqq$ 0.95), which means the object is very likely to be a point source, in addition to the same conditions, i.e., (1), (2), and (3). Figure 3 shows an example of the effect of this requirement. Likely point sources except for the other type of sources such as galaxies and nebulas are remained. The sources located at the edge of y-axis are roughly excluded in order to avoid the possible effects of distortion due to the optics, i.e., y $\leqq$ 500 in Chip2, Chip3, Chip6, Chip7, and Chip8, or y $\geqq$ 3,500 in Chip0, Chip1, Chip4, Chip5, and Chip9. The frames which contain less than 5 effective objects are also not used in the following analysis. According to the above criteria, the numbers of shots are 5,161, 5,315, and 5,122 for the Rc, i', and z' filters, respectively.

In each shot, only the frames of Chip2 (DET-ID = 2) and Chip5 (DET-ID = 5), which are located at the center of the field of view, are used for the following PSF evaluations in order to reduce distortion effect. The CCD layout is shown in figure 4. In the following sections, we regard the mean of mode of PSF size (or ellipticity) in Chip2 and Chip5 as the representative value of PSF size (or ellipticity) of each shot in

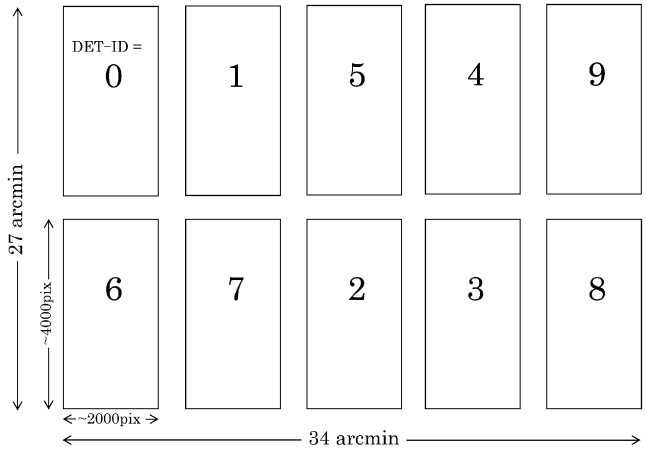


**Fig. 4.** The layout of 10 CCDs (MIT/LL) of Suprime-Cam.

this study. Here, we use the bin size of 0.01 in the mode calculation. The shots in the absence of frames of Chip2 or Chip5 are excluded. Mean value is adopted if the number of frames in bins are same. Finally, the mode values of PSF size and ellipticity for 5,105, 5,208, and 5,029 of the shots are calculated for Rc, i' and z' filters, respectively. Here, the difference of CCD sensitivity between the center of a CCD chip and the edge of the discussed area (Y = 500 in Chip2, and Y = 3500 in Chip5) is approximately 5%. Therefore we consider that the difference is small enough to use raw data in the following analysis.

## 4. Results and Discussion

Among the selected shots, the characteristics are discussed using the shots with zenith distance ≦ 50 degrees. This value is limited because minimum value of PSF size is growing larger with larger zenith distance (see figure 5). This tendency is seen more remarkably in the case of a shorter wavelength pass filter. Since the number of frames at each zenith distance is also considered, we adopt 50 degrees in this paper. Moreover, we require the shots with ellipticity (ELLIPTICITY, given by SExtractor with 1-B/A) of ≦ 0.4. The small ellipticity means a round shape. This condition excludes shots including extremely elongated PSF sources which may be due to tracking and/or guiding errors. In figure 6, we found that a range of three-sigma error is large, when a number of detected stars in a frame is less than 30. Therefore, we exclude shots, in which detected a number of sources in Chip2 and Chip5 are less than 30.

Figure 7a and 7b give differences of determined PSF mode between Chip2 and Chip5 in a same shot. The zero value in the horizontal axis gives no difference between Chip2 and Chip5. In figure 7a, the histograms indicate that the mode of PSF size in Chip2 is slightly (0.02 arcsec) smaller than that in Chip5. In figure 7b, it is shown that the differences of the mode of ellipticity are small. Also we examined that the PSF mode between Chip2 and Chip5 does not depend on the difference in the number of sources on each frame. For example, in the case of large difference of 2,726 sources between Chip2 and Chip5 (SUPA00225722 and SUPA00225725), the differences are 0.01 arcsec in the PSF size and 0.02 in the ellipticity (0.46 arcsec and 0.07 in Chip2 and 0.45 arcsec and 0.05 in Chip5), respectively. However, such a large difference in the source number is an uncommon case. Therefore, we use the mean of PSF mode for PSF evaluations in this study.

Hereafter, we examine the characteristics of seasonal variation in a year, long-term variation and time variation during a night in the PSF of the Suprime-Cam data for 7 years using the mean in a month, a year, and a night with a three sigma cut, respectively. The number of shots discussed in the following is 3,225, 3150, and 2385 for Rc, i', and z' filters, respectively. These shots have zenith distance ≦ 50, ellipticity ≦ 0.4 and the number of point sources in Chip2 and Chip5 ≧ 30. Table 1 summarizes the number of shots passed through the selections which are described in section 2 and section 3.

In the following figures, the simple mean values of PSF size measured from AG about every 1 minute during 5UT to

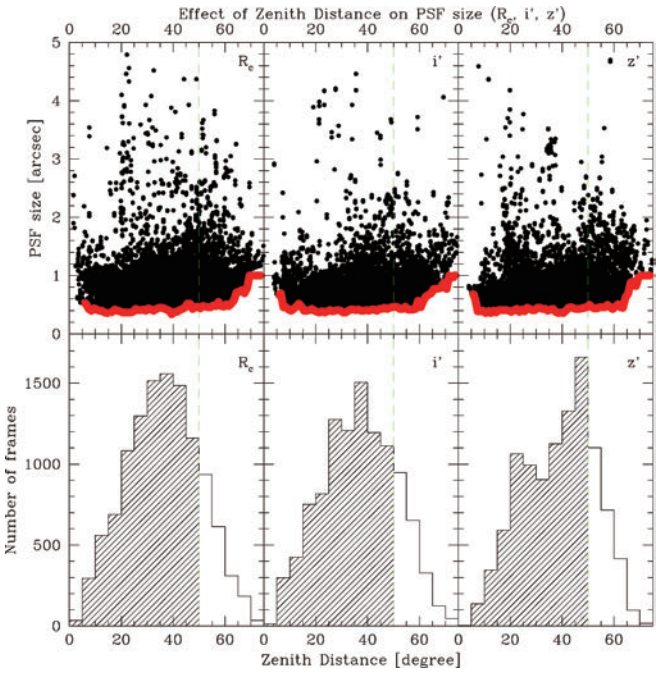


**Fig. 5.** The distributions of PSF size as a function of zenith distance (upper 3 panels) and the histograms of the number of frames (lower 3 panels) for the Rc (left), i' (middle), and z' (right) bands. The red curves depict the minimum PSF size at each zenith distance. The vertical dashed lines indicate the upper limit of zenith distance for the following analysis. The bin size of histograms is set to 5 degrees.

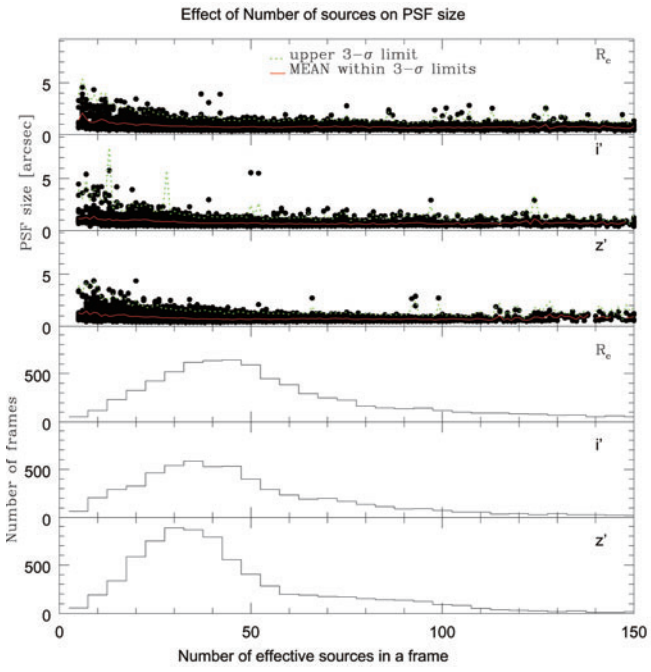


**Fig. 6.** The distribution of PSF size as a function of the number of sources in each frame (upper 3 panels) and the histogram of the number of frames (lower 3 panels). The data are categorized by Rc, i', and z' bands. The dashed green curves show the upper three-sigma limit as a function of the number of sources. The solid red curves show the mean value of PSF size within three-sigma limits. The bin size of histograms is defined to be 5.

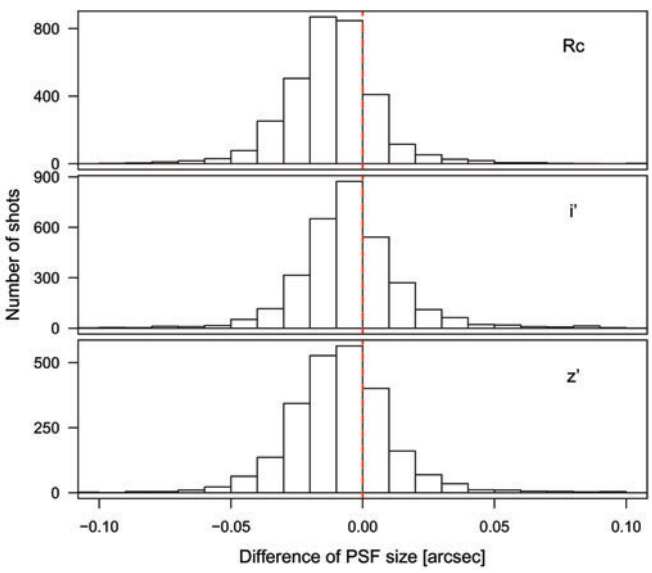


**Fig. 7a.** The histogram of the difference of PSF size between Chip2 and Chip5. The vertical axis gives the number of shots in Chip2. The horizontal axis gives by (the mode of PSF size in Chip2) - (the mode of PSF size in Chip5). The red dashed lines indicate the zero (no difference).

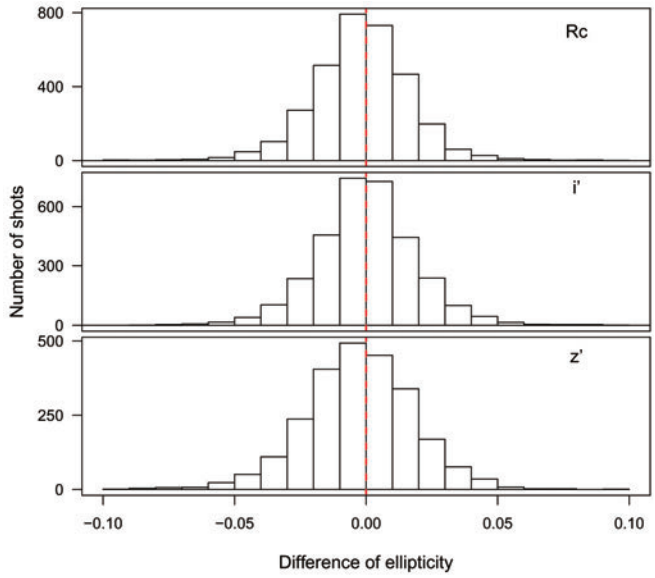


**Fig. 7b.** The histogram of the difference of ellipticity between Chip2 and Chip5. The vertical axis gives the number of shots in Chip2. The horizontal axis gives by (the ellipticity in Chip2) - (the ellipticity in Chip5). The red dashed lines indicate the zero (no difference).

**Table 1.** The summarize of the data selections. The number in each filter indicates the number of observed shot. N2 and N5 indicate the number of sources which are detected in Chip2 and Chip5, respectively.

| filter<br>description of selections | Rc | i' | z' |
|---|---|---|---|
| (1) May 2001-June 2008 | 7,336 | 6,695 | 6,646 |
| (2) 'Data type' and 'Object Name' restriction | 5,315 | 5,504 | 5,238 |
| (3) after the 2nd SExtractor | 5,161 | 5,315 | 5,122 |
| (4) exist images on both Chip 2 and Chip 5 | 5,105 | 5,208 | 5,029 |
| (5) zenith distance $\leqq$50, ellipticity $\leqq$0.4, N2 $\geqq$30 and N5 $\geqq$30 | 3,225 | 3,150 | 2,385 |

15UT are shown. The data points using here do not indicate the real PSF size because the AG star images are often taken under slightly off-focus condition. Therefore, the PSF size from AG is a only reference to compare with the results from Miyashita et al. (2004). The PSF size from AG can be browsed on a dedicated SMOKA web page[5]. PSF size from DIMM (Differential Image Motion Monitor, Uraguchi et al. 2006, the wavelength range is 300 - 1,100 nm) obtained at the outside of the dome of Subaru Telescope are also archived in SMOKA, but we do not use it because the operation period of DIMM system is very short (April 2006 to December 2007).

[5] http://smoka.nao.ac.jp/calendar.jsp

### *4.1 Seasonal Characteristics*

In figure 8, the seasonal characteristics of the PSF are shown. The top panel gives variations of the mean PSF sizes for the Rc, i' and z' filters. The PSF sizes in the all filters show a similar trend, where the PSF size is smaller around September rather than around March. In particular, the mean PSF size around March is distributed about 0.8 arcsec, and less than 0.7 arcsec in August - October. The smallest PSF size from AG is seen in September, whereas the worst is seen in March. This feature is the same as the result by Miyashita et al. (2004).

The middle panel shows characteristics of the ellipticity. In contrast to the PSF sizes, the ellipticities in the Rc and z' filters are larger in the latter half of a year. There is no clear seasonal trend in the ellipticity in the i' filter. We examined the

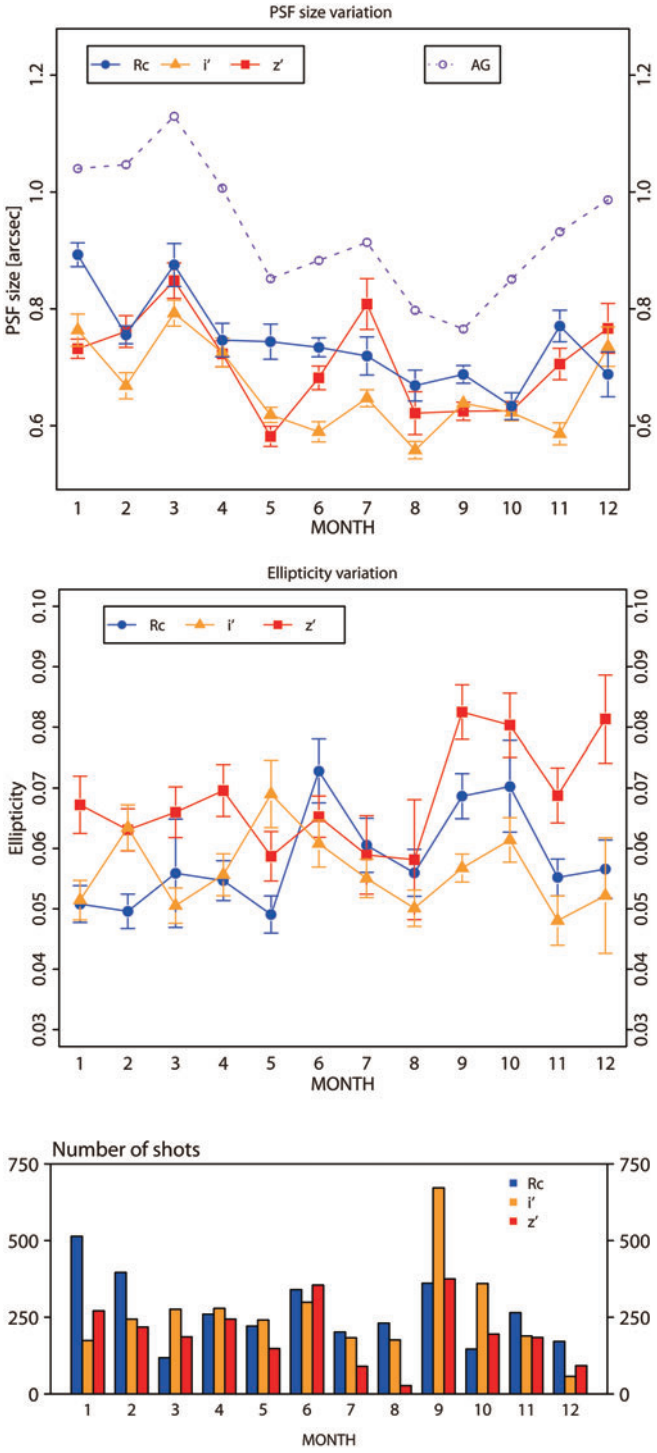


**Fig. 8.** The seasonal variations in the PSF. The top panel, data points indicate the average PSF size in a month which are derived by clipping outlying data points with a three sigma cut. The middle panel gives the ellipticity variation. The error bars indicate their 95% confidence intervals. Here, it is assumed that a distribution of the seeing size is based on the normal distribution. We set the lower probability value of t-distribution to 0.975. In the both panels, the red, orange and red colors indicate the mean value of Rc, i' and z' in each month, respectively. The PSF size from AG are also plotted with open purple circle in the top panel. The bottom panel gives the number of shots in each month.

correlations between the PSF size and the ellipticity in the three filters, however no clear correlation was found (see figure 9).

The bottom panel in figure 8 shows the number of shots in each month. The number of shots in Rc is larger than those in i' and z' in the winter season. On the other hand, the number of shots in i' and z' in September - October is much larger than that in Rc.

We show in figure 10 the fraction of shots whose mean

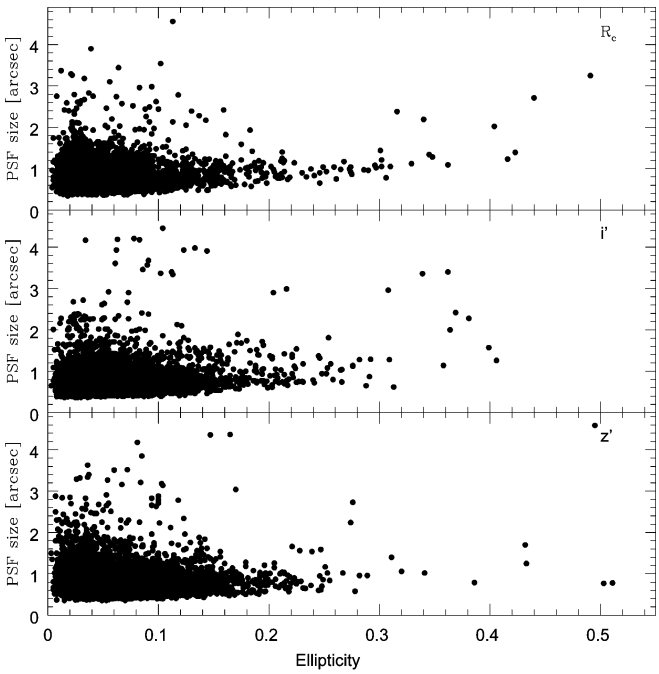


**Fig. 9.** The PSF size distribution as a function of ellipticity.

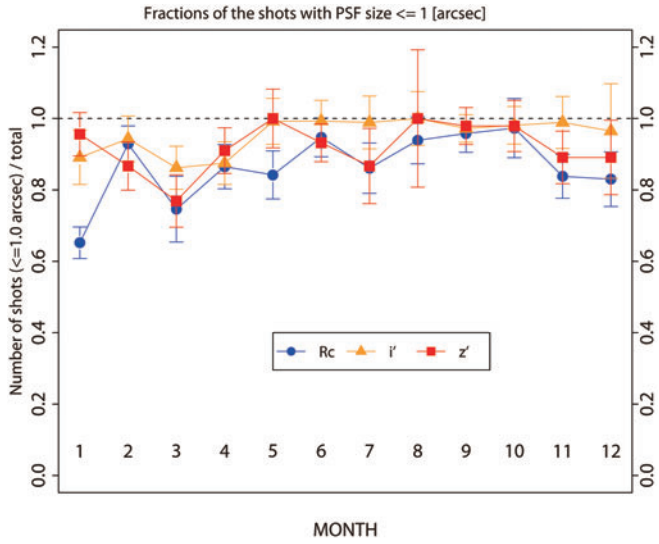


**Fig. 10.** The fractions of the shots whose PSF sizes are smaller than 1 arcsec in each month. The symbols indicate the same as in figure 8.

PSF size in a month is smaller than 1 arcsec. In this figure, we find that the mean PSF sizes in most of the shots (more than 95%) are smaller than 1 arcsec in September - October in Rc, May - December in i', and January, May, August - October in z'. On the other hand, the fractions of the shots in March which satisfy the mean PSF size of < 1 arcsec are smaller than 0.87 for the three filters. This is the second-worst month for the Rc filter, and the worst month for the i' and z' filters in terms of the seeing condition. The smallest fraction of all is 0.65, in January with the Rc filter.

In figure 11a, b, c, we show the PSF size distribution in March (upper panel), August (middle panel), and October (bottom panel) for the three filters. The distribution peak is at around 0.5-0.6 arcsec for Rc and i', and 0.6-0.7 arcsec for z' in August and October. On the other hand, the peak is at around 0.7 arcsec for Rc and i', and 0.6-0.8 arcsec for z' in March. To summarize, we find that the PSF size is likely to be smaller in August and October rather than in March through a year.

### *4.2 Long-term Characteristics*

Figure 12 shows the result of the long-term variations in the mean PSF in each year for the three filters. In the upper-left panel, the PSF size of Rc gently decreases from 2002 to 2005, and from 2006 to 2008, whereas the z' and i' filters do not show a long-term decreasing trend. They increase from 2003 to 2004, and from 2006 to 2007, instead. The PSF size of i' also increases in 2005. Continuous increase in the PSF size from AG is found. This variation in the case of AG may be due to the modification of the seeing calculation algorithm or potential mechanical problems in 2004 according to the private communication with Dr. George Kosugi. However, the cause is uncertain.

The upper-right panel gives the long-term characteristics of ellipticity. It is possible that ellipticity changes due to the telescope tracking and the altitude of the object. The ellipticities in the three filters decrease from 2002 to 2005 except for i' in 2003 and Rc in 2004. They in the Rc and z' filters increase in 2006, whereas they in the i' filter gently decrease to 2007.

The lower panel shows the number of shots. The total number of shots in each year decreases from 2002 to 2006. The largest number of shots is taken with the Rc and i' filters in 2002, and with the z' filter in 2004.

When we compare the upper panels, there is no significant common trend in the PSF size and ellipticity among filters. On the other hand, the pair of filters which show similar trends in the variations in the PSF after 2005 is different between for the PSF size and for the ellipticity. The trends of the PSF size after 2005 are similar in i' and z',

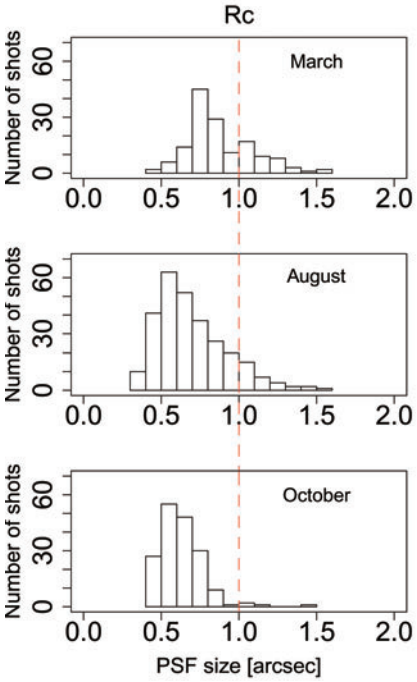


**Fig. 11a.** Examples of the PSF size distribution of Rc in March, August and October is shown. The vertical dashed line shows the PSF size of 1 arcsec.

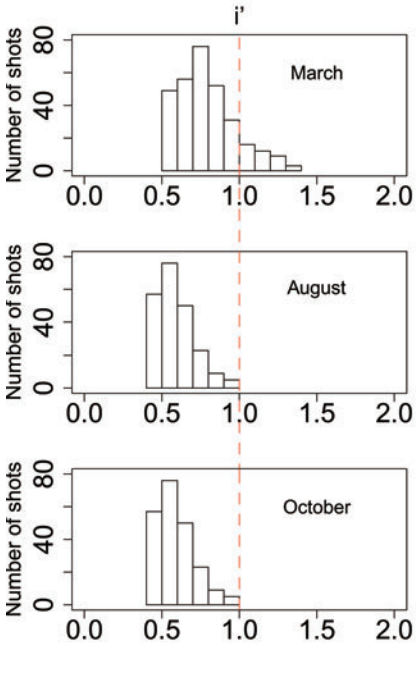


**Fig. 11b.** Examples of the PSF size distribution of i' in March, August and October.

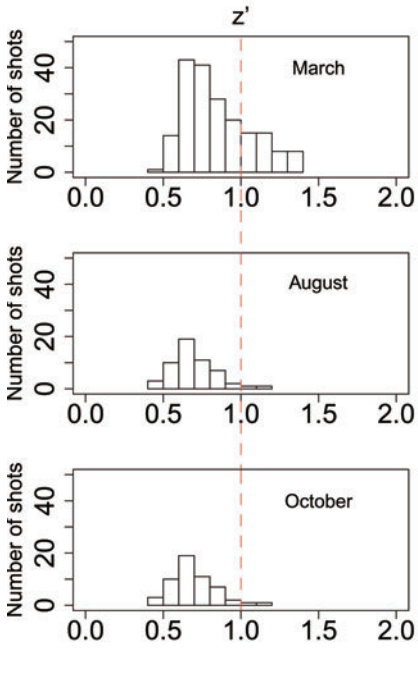


**Fig. 11c.** Examples of the PSF size distribution of z' in March, August, and October.

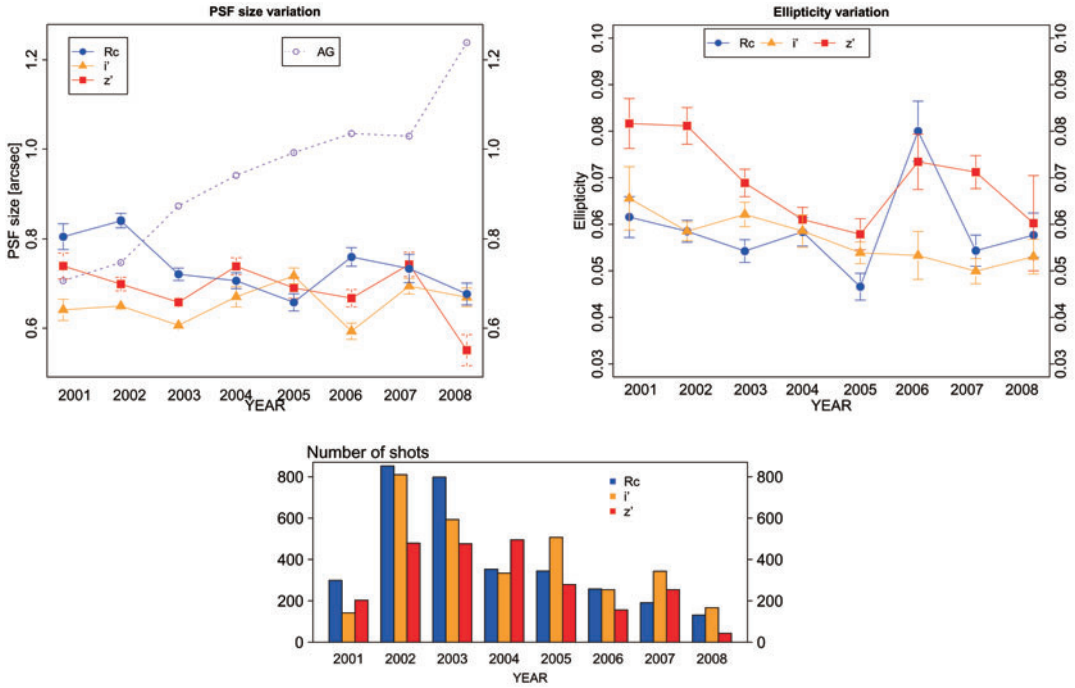


**Fig. 12.** The long-term variations in the PSF. The upper-left panel gives the PSF size of three filters and AG. The symbols and error bars are assigned in the same manner as in figure 8. The upper-right panel gives the ellipticity variation. The symbols and error bars indicate the same as in figure 8. The lower panel shows the number of shots in each year.

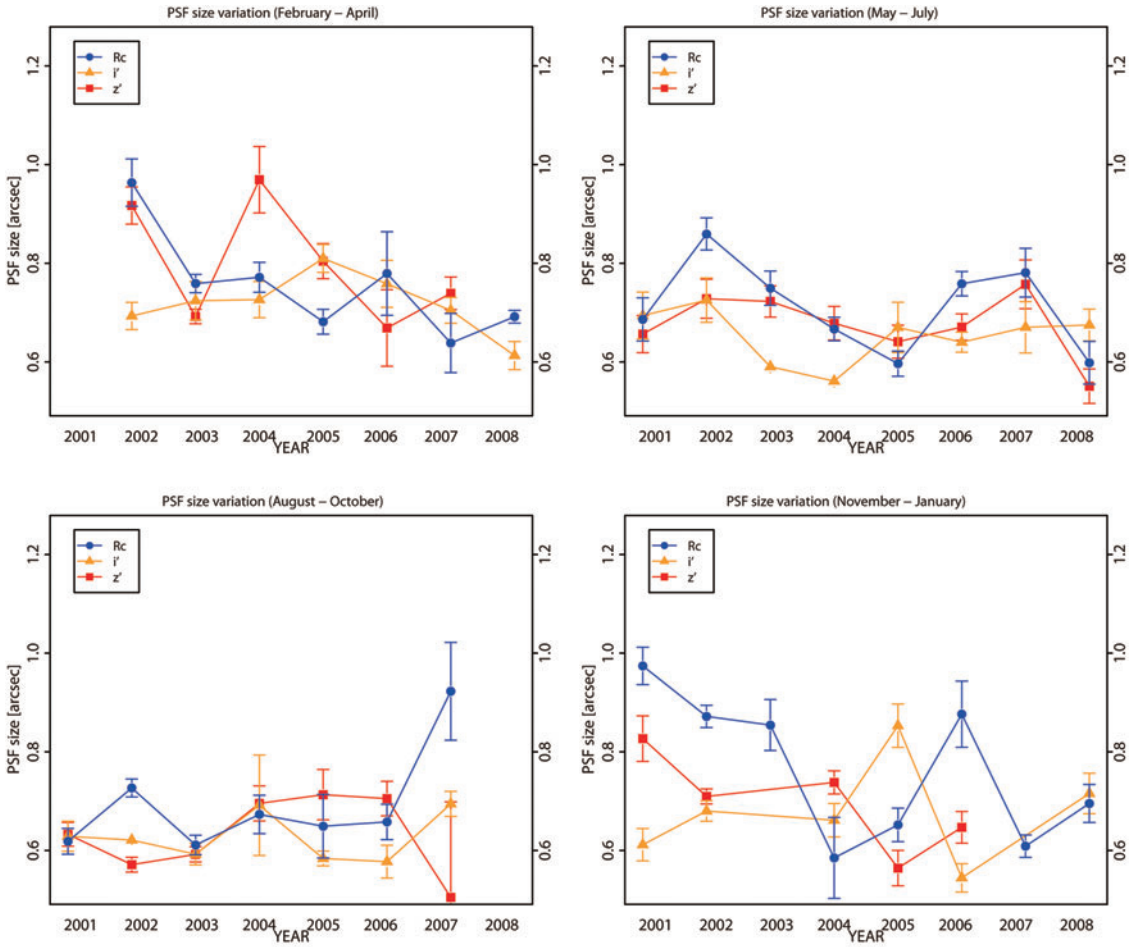


**Fig. 13.** The long-term variations of the PSF size for the four periods, February - April, May - July, August - October, and November - January.

whereas those of the ellipticity from 2005 to 2007 are similar in Rc and z'.

Such trends may be mainly due to the change of the atmospheric condition, although they may be results of the complex factors. For example, observers may change filters or targets, or stop observations due to weather conditions or instrument troubles. It is not easy to specify the main factors of such trends. In order to take various cases into account, more detail analysis using not only using FITS header information but also observation logs. We note that we only have the logs since November 2004.

The seasonal variation of PSF size shows remarkable trend as described in section 4.1. In order to discuss effects of seasonal variation on the long-term trends of PSF size, we divide twelve months into four periods, i.e., February - April, May - July, August - October, and November - January. Figure 13 gives the long-term variations of the PSF size for the four seasons. The distribution of PSF size in August - October until 2006 is clearly smaller than those in the other seasons. The decreasing trend from 2002 to 2005 in the Rc filter, as mentioned in section 4.1, would be affected by the three seasons except August - October.

### *4.3 Nightly Time-to-Time Characteristics*

In figure 14, we present the time variation in the PSF during the observing night and the number of shots in each hour. In the upper-left panel, the PSF size of z' is not stable for several hours in the early observation night, however, they tend to become smaller values from 12UT to 13UT. The PSF size in the Rc and i' filters also become small at 12UT although they are comparatively stable in the early observation night. In general, the seeing condition possibly deteriorates just after the opening of the dome shutter because of the difference in temperatures between in and outside the dome, and of the consequent instability of airflows in the dome. The PSF size in the z' filter may indicate the effect. The PSF size in the i' filter gently becomes smaller from 5UT and increases from 13UT. The PSF size from AG moderately decreases in the early observation night, then increases at 15UT as similar to the trend seen in the i' filter. Such increase feature is also found in the three filters. It is necessary to pay attention to the fact that we do not take into account unspecified artificial factors such as intervals of re-adjusting focus. This may differ from observer to observer and from time to time.

The ellipticity variation is also given in the upper-right

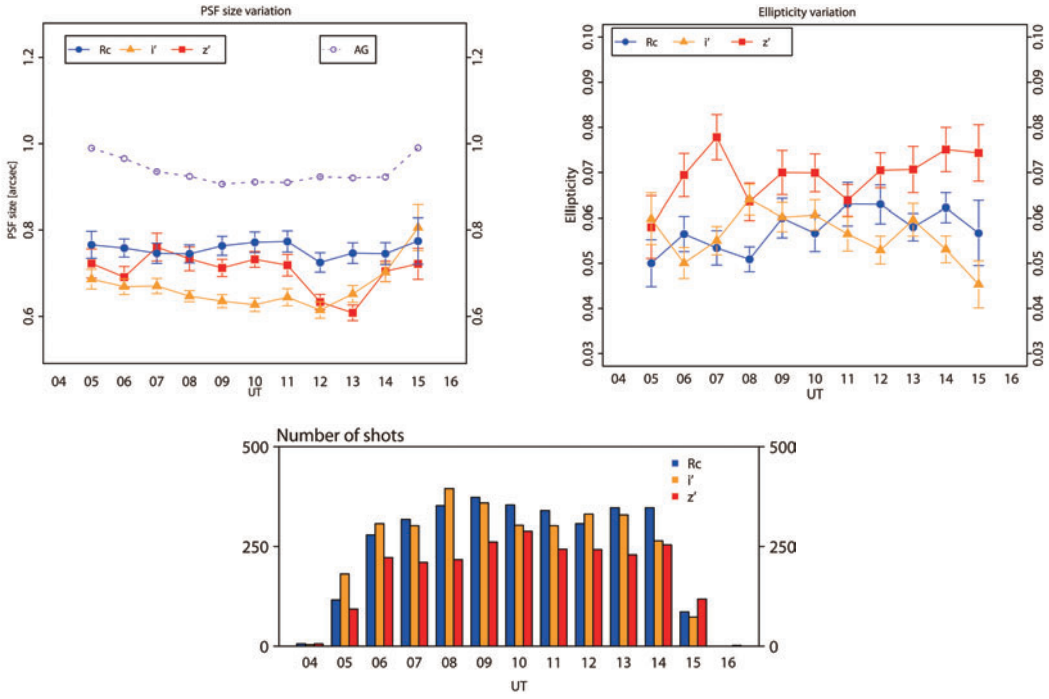


**Fig. 14.** The time variation in the PSF during the night. The upper-left panel gives the PSF size of three filters and AG. The symbols and error bars indicate the same meanings as in figure 8. The horizontal axis, UT (UT - HST = 10), indicates the starting UTC of the exposure derived from the FITS header. The upper-right panel shows the time variations of ellipticity. The lower panel gives the number of shots in each hour. The shots of 4UT and 16 in the upper panels are not plotted because of the extremely poor number of shots as seen in the bottom panel.

panel of figure 14. There is no clear common trend among filters in ellipticity characteristics except for the decrease in the early morning. Such small ellipticity and large PSF size may indicate possible recurring off-focus imaging every night in the morning hours. More detail analysis needs to confirm this presumption.

In the lower panel, we can find that the i' filter is used in the beginning of the observations (5UT and 6UT). On the other hand, the Rc filter is used in the middle of the night (9UT to 11UT).

The time variations of the PSF size during the four seasons examined as section 4.2 are shown in figure 15. As same as the long-term variation, the distribution of PSF size in August - October is smaller than the other three seasons except at around 12UT. In this season, the PSF size in the z' filter is smaller in the latter half of the night. The increase trend in the early morning can be seen in all seasons for the z' filter, also for the i' filter except November - January although the error bars are large. To summarize, the PSF size and the distribution in August - October are smaller than the other three seasons.

## 5. Summary

We investigate the trends in PSF characteristics of the Subaru/Suprime-Cam data. The shots with zenith distance ≦ 50 degrees and ellipticity ≦ 0.4 of the Rc, i', and z' filters show that the seasonal characteristics indicate the PSF size is smaller from August to October, whereas larger from February to April. This results support the results of AG seasonal trends from Miyashita et al. (2004). In long-term characteristics, there are no common trends among the three filters.

The PSF size for the z' filter is smaller in the latter half of the night. Also the PSF sizes in the three filters become larger in the early morning. The results in this study may support the trends which many observers using Suprime-Cam have felt somehow or other with no verification in a statistical manner. It is necessary to pay attention to many artificial factors such as focusing intervals, habits of observers and

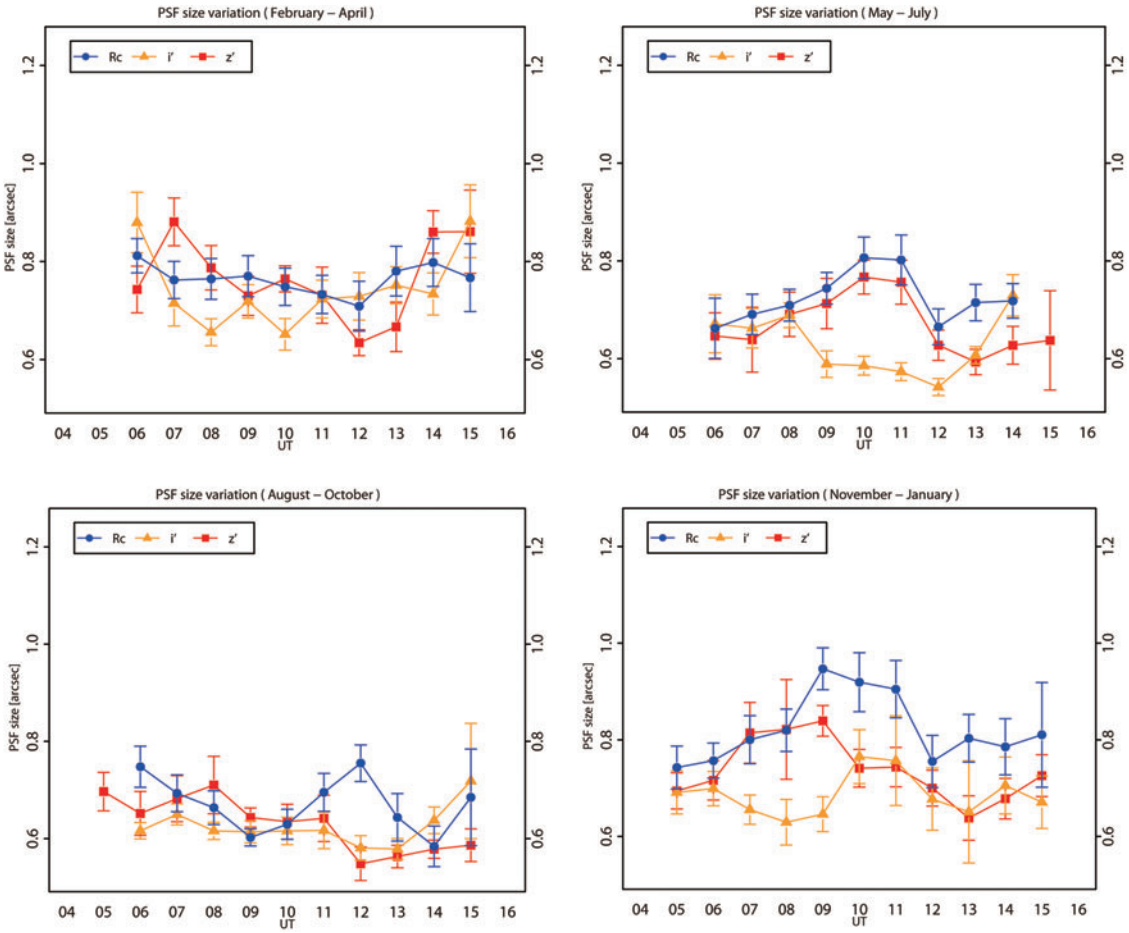


**Fig. 15.** The time-to-time variations of the PSF size for the four periods, February - April, May - July, August - October, and November - January.

tendencies in observed objects. The relevance of the trends in PSF will be investigate with weather data in a future work.

We would like to thank Dr. Masafumi Yagi, Prof. Koji Ohta and Prof. Michitoshi Yoshida for their helpful discussions and comments upon our study. We also thank Dr. George Kosugi and Mr. Fumihiro Uraguchi for their useful information and suggestions on our data analysis. We are grateful to an anonymous referee for a careful reading the original manuscript and beneficial prompting to improve this paper.

**References**

Baba, H., Yasuda, N., Ichikawa, S., Yagi, M., Iwamoto, N., Takata, T., Horaguchi, T., Taga, M., Watanabe, M., Okumura, S., Ozawa, T., Yamamoto, N., and Hamabe, M. 2002, "Development of public science archive system of Subaru Telescope", RNAOJ., 6, 23-36

Bertin, E., and Arnouts, S. 1996, "SExtractor: Software for source extraction" Astron. Astrophys. Suppl., 117, 393-404

Enoki, M., Taga, M., Ozawa, T., Noda, S., Okumura, S., Yoshino, A., Furusho, R., Baba, H., Horaguchi, T., Takata, T., and Ichikawa, S. 2004, "Development of public science archive system of Subaru Telescope 3", RNAOJ., 7, 57-84

Ideta, M., Enoki, M., Ozawa, T., Yoshino, A., Nakata, F., Okumura, S., Yamamoto, N., Furusho, R., Yaji, K., Yamada, Y., Yagi, M., Horaguchi, T., Takata, T., and Ichikawa, S. 2005, "Development of public science archive system of Subaru Telescope 4", RNAOJ., 8, 59-84

Kaifu, N. 1998, "SUBARU Telescope", Advanced Technology Optical/IR Telescopes VI, Edited by Stepp, L.M., SPIE, Vol. 3352, 14-22

Kotani T., Kawai N., Yanagisawa K., Watanabe J., Arimoto M., Fukushima H., Hattori T., Inata M., Izumiura H., Kataoka J., Koyano H., Kubota K., Kuroda D., Mori M., Nagayama S., Ohta K., Okada T., Okita K., Sato R., Serino Y., Shimizu Y., Shimokawabe T., Suzuki M., Toda H., Ushiyama T., Yatsu Y., Yoshida A., and Yoshida M. 2005, "MITSuME - Multicolor Imaging Telescopes for Survey and Monstrous Explosions", Il Nuovo Cimento C, 28, 755

Miyashita, A., Takato, N., Usuda, T., Uraguchi, F., and Ogasawara, R. 2004, "Statistics of weather data, environmental data and the seeing of the Subaru Telescope", Ground-based Telescopes. Edited by Jacobus M. Oschmann, Jr., SPIE, Vol. 5489, 207-217

Miyazaki, S., Komiyama, Y., Sekiguchi, M., Okamura, S., Doi, M., Furusawa, H., Hamabe, M., Imi, K., Kimura, M., Nakata, F., Okada, N., Ouchi, M., Shimasaku, K., Yagi, M., and Yasuda, N. 2002, "Subaru Prime Focus Camera – Suprime-Cam", PASJ, 54, 833-853

Nakata, F., Ideta, M., Yagi, M., Enoki, M., Yoshino, A., Yamada, Y., Takata, T., and Ichikawa, S. 2005, "Development of Quality Assessment System for Observed Data Obtained by the Subaru Telescope", Report of the National Astronomical Observatory of Japan, Vol.8, 43-57

Uemura M., Arai A., and Uehara T. 2006, "GRB 061121: optical observation at the KANATA 1.5m telescope", GRB Coordinates Network, Circular Service, 5828, 1

Uraguchi, F., Takato, N., Miyashita, A., and Usuda, T. 2006, "The DIMM station at Subaru Telescope", Ground-based and Airborne Telescopes. Edited by Stepp, L.M., SPIE, Vol. 6267, 21-30

Yamada Y., Ozawa, T., Nishizawa A., Furusho R., Nishimura T., Enoki M., Yoshino A., Furusawa J., Takata T., and Ichikawa S. 2009, "Development of public science archive system of Subaru Telescope. 5", RNAOJ, 12, 53-78

Yamamoto, N., Noda, S., Taga, M., Ozawa, T., Horaguchi, T., Okumura, S., Furusho, R., Baba, H., Yagi, M., Yasuda, N., Takata, T., and Ichikawa, S. 2003, "Development of public science archive system of Subaru Telescope. 2", RNAOJ., 6, 79-100